Measuring sickle cell morphology during blood flow

Inna Kviatkovsky,[1] Adel Zeidan,[1] Daniella Yeheskely-Hayon,[1] Eveline L. Shabad,[2] Eldad J. Dann,[2,3] and Dvir Yelin[1]

[1]Faculty of Biomedical Engineering, Technion - IIT, Haifa, Israel
[2]Department of Hematology and Bone Marrow Transplantation, Rambam Medical Center, Haifa, Israel
[3]Bruce Rappaport Faculty of Medicine, Technion -ITI Haifa, Israel
*yelin@bm.technion.ac.il

Abstract: During a sickle cell crisis in sickle cell anemia patients, deoxygenated red blood cells may change their mechanical properties and block small blood vessels, causing pain, local tissue damage, and possibly organ failure. Measuring the structural and morphological changes in sickle cells is important for understanding the factors contributing to vessel blockage and for developing an effective treatment. In this work, we image blood cells from sickle cell anemia patients using spectrally encoded flow cytometry, and analyze the interference patterns between reflections from the cell membranes. Using a numerical simulation for calculating the interference pattern obtained from a model of a red blood cell, we propose an analytical expression for the three-dimensional shape of characteristic sickle cells and compare our results to a previously suggested model. Our imaging approach offers new means for analyzing the morphology of sickle cells, and could be useful for studying their unique physiological and biomechanical properties.

References and links

1. L. Pauling, H. A. Itano, S. Singer, and I. Wells, "Sickle Cell Anemia a Molecular Disease," Science **110**(2865), 543–548 (1949).
2. V. M. Ingram, "Gene mutations in human haemoglobin: the chemical difference between normal and sickle cell haemoglobin," Nature **180**(4581), 326–328 (1957).
3. R. E. Samuel, E. D. Salmon, and R. W. Briehl, "Nucleation and growth of fibres and gel formation in sickle cell haemoglobin," Nature **345**(6278), 833–835 (1990).
4. G. W. Christoph, J. Hofrichter, and W. A. Eaton, "Understanding the shape of sickled red cells," Biophys. J. **88**(2), 1371–1376 (2005).
5. L. W. Diggs, and J. Bibb, "The erythrocyte in sickle cell anemia: Morphology, size, hemoglobin content, fragility and sedimentation rate," J. Am. Med. Assoc. **112**(8), 695–701 (1939).
6. R. P. Hebbel, O. Yamada, C. F. Moldow, H. S. Jacob, J. G. White, and J. W. Eaton, "Abnormal adherence of sickle erythrocytes to cultured vascular endothelium: Possible mechanism for microvascular occlusion in sickle cell disease," J. Clin. Invest. **65**(1), 154–160 (1980).
7. R. Hoover, R. Rubin, G. Wise, and R. Warren, "Adhesion of normal and sickle erythrocytes to endothelial monolayer cultures," Blood **54**(4), 872–876 (1979).
8. O. S. Platt, D. J. Brambilla, W. F. Rosse, P. F. Milner, O. Castro, M. H. Steinberg, and P. P. Klug, "Mortality In Sickle Cell Disease. Life Expectancy and Risk Factors for Early Death," N. Engl. J. Med. **330**(23), 1639–1644 (1994).
9. G. A. Barabino, L. V. McIntire, S. G. Eskin, D. A. Sears, and M. Udden, "Endothelial cell interactions with sickle cell, sickle trait, mechanically injured, and normal erythrocytes under controlled flow," Blood **70**(1), 152–157 (1987).
10. E. Evans, N. Mohandas, and A. Leung, "Static and dynamic rigidities of normal and sickle erythrocytes. Major influence of cell hemoglobin concentration," J. Clin. Invest. **73**(2), 477–488 (1984).
11. J. L. Maciaszek, B. Andemariam, and G. Lykotrafitis, "Microelasticity of red blood cells in sickle cell disease," J. Strain Anal. Eng. Des. **46**(5), 368–379 (2011).
12. N. T. Shaked, L. L. Satterwhite, M. J. Telen, G. A. Truskey, and A. Wax, "Quantitative microscopy and nanoscopy of sickle red blood cells performed by wide field digital interferometry," J. Biomed. Opt. **16**(3), 030506 (2011).

13. H. Byun, T. R. Hillman, J. M. Higgins, M. Diez-Silva, Z. Peng, M. Dao, R. R. Dasari, S. Suresh, and Y. Park, "Optical measurement of biomechanical properties of individual erythrocytes from a sickle cell patient," Acta Biomater. **8**(11), 4130–4138 (2012).
14. T. Asakura, J. A. Mattiello, K. Obata, K. Asakura, M. P. Reilly, N. Tomassini, E. Schwartz, and K. Ohene-Frempong, "Partially oxygenated sickled cells: Sickle-shaped red cells found in circulating blood of patients with sickle cell disease," Proc. Natl. Acad. Sci. U.S.A. **91**(26), 12589–12593 (1994).
15. D. K. Kaul, M. E. Fabry, P. Windisch, S. Baez, and R. L. Nagel, "Erythrocytes in Sickle Cell Anemia Are Heterogeneous in Their Rheological and Hemodynamic Characteristics," J. Clin. Invest. **72**(1), 22–31 (1983).
16. Y. Sung, N. Lue, B. Hamza, J. Martel, D. Irimia, R. R. Dasari, W. Choi, Z. Yaqoob, and P. So, "Three-Dimensional Holographic Refractive-Index Measurement of Continuously Flowing Cells in a Microfluidic Channel," Phys. Rev. Appl. **1**(1), 014002 (2014).
17. K. Kim, K. S. Kim, H. Park, J. C. Ye, and Y. Park, "Real-time visualization of 3-D dynamic microscopic objects using optical diffraction tomography," Opt. Express **21**(26), 32269–32278 (2013).
18. G. Tomaiuolo, "Biomechanical properties of red blood cells in health and disease towards microfluidics," Biomicrofluidics **8**(5), 051501 (2014).
19. X. Li, M. Dao, G. Lykotrafitis, and G. E. Karniadakis, "Biomechanics and biorheology of red blood cells in sickle cell anemia," J. Biomech. **50**, 34–41 (2017).
20. L. Golan and D. Yelin, "Flow cytometry using spectrally encoded confocal microscopy," Opt. Lett. **35**(13), 2218–2220 (2010).
21. L. Golan, D. Yeheskely-Hayon, L. Minai, E. J. Dann, and D. Yelin, "Noninvasive imaging of flowing blood cells using label-free spectrally encoded flow cytometry," Biomed. Opt. Express **3**(6), 1455–1464 (2012).
22. A. Zeidan and D. Yelin, "Reflectance confocal microscopy of red blood cells: simulation and experiment," Biomed. Opt. Express **6**(11), 4335–4343 (2015).
23. H. Lei and G. E. Karniadakis, "Quantifying the rheological and hemodynamic characteristics of sickle cell anemia," Biophys. J. **102**(2), 185–194 (2012).
24. X. Li, P. M. Vlahovska, and G. E. Karniadakis, "Continuum- and particle-based modeling of shapes and dynamics of red blood cells in health and disease," Soft Matter **9**(1), 28–37 (2013).
25. Z. Huang, L. Hearne, C. E. Irby, S. B. King, S. K. Ballas, and D. B. Kim-Shapiro, "Kinetics of increased deformability of deoxygenated sickle cells upon oxygenation," Biophys. J. **85**(4), 2374–2383 (2003).
26. M. Stücker, V. Baier, T. Reuther, K. Hoffmann, K. Kellam, and P. Altmeyer, "Capillary blood cell velocity in human skin capillaries located perpendicularly to the skin surface: measured by a new laser Doppler anemometer," Microvasc. Res. **52**(2), 188–192 (1996).
27. R. Ashcroft, "Oh's Intensive Care Manual, 7th Edition," Can. J. Anesth. Can. Anesth. **62**, 1026 (2015).
28. B. Wranne, R. D. Woodson, and J. C. Detter, "Bohr Effect: interaction between H $^+$, CO_2, and 2,3-DPG in fresh and stored blood," J. Appl. Physiol. **32**(6), 749–754 (1972).
29. M. Bessis, R. Weed and P. Leblond, *Red Cell Shape* (Springer, 1973).
30. B. E. Glader, R. D. Propper, and G. R. Buchanan, "Microcytosis Associated with Sickle Cell Anemia," Am. J. Clin. Pathol. **72**(1), 63–64 (1979).
31. E. Evans and Y. C. Fung, "Improved Measurements of the Erythrocyte Geometry," Microvasc. Res. **4**(4), 335–347 (1972).
32. V. Bennett, "The spectrin-actin junction of erythrocyte membrane skeletons," Biochim. Biophys. Acta **988**(1), 107–121 (1989).

1. Introduction

Sickle cell anemia is a molecular disease [1] in which the hemoglobin molecular structure is altered due to a change in a single amino acid in the Hemoglobin beta chain [2]. When exposed to low oxygen pressure, the abnormal molecules tend to aggregate and polymerize [3], causing morphological changes [4] in the red blood cells of sickle cell anemia patients. The polymerization process is highly dependent on hemoglobin concentration and deoxygenation rates [5], resulting in a wide variety of cell deformations. In addition to morphological changes, hemoglobin polymerization also affects the cells' mechanical properties, including reduced membrane elasticity and lower extracellular exposure of adhesion molecules [6,7]. These cellular modifications could eventually cause vessel occlusion that could result in pain, local tissue damage, and in some cases may lead to organ failure and even death due to stroke or acute chest syndrome [8].

Measuring sickle cell mechanical properties using the parallel plate flowing method [9] and pipette aspiration [10] have allowed researchers to characterize the rheological properties of blood from sickle cell anemia patients, while advanced imaging modalities including atomic force microscopy [11] and optical interferometry [12,13] have been used to study the pathophysiology of this disease. With most conventional microscopy techniques, however,

red blood cells are often immobilized and imaged in contact with a supportive solid surface [12,14,15]. Evidently, imaging the cells suspended within a liquid or in flow would provide a more clinically relevant environment for studying the cells' morphology and mechanical properties. Microfluidics have recently emerged as a powerful method for evaluation of various properties of flowing red blood cells [16,17]. Parameters including cell volume, surface area and other biomechanical properties were analyzed in blood from healthy and ill patients [18,19]. The conventional widefield, phase-contrast and holographic microscopy techniques used in these works; however, lack optical sectioning capabilities and are often less effective for imaging large numbers or dense populations of cells. High-resolution imaging of red blood cells in flow has recently become possible using spectrally encoded flow cytometry (SEFC) [20,21] that employs space encoding by wavelength for confocal imaging of reflections along a single transverse line within a vessel. Our group has demonstrated confocal imaging of flowing red and white blood cells, both *in vitro* [20] and *in vivo* [20], without mechanical scanning, where one axis is encoded by wavelength and the other axis is encoded by time. Additional information on the cell morphology in three-dimensions was obtained from the SEFC images by analyzing the interference patterns resulting from reflections from the front and back plasma membranes [22]. In this work, we use our SEFC system to image and analyze blood cells obtained from sickle cell anemia patients. Our results reveal that the cells three-dimensional shapes in flow differ from those reported previously [23,24], and propose a new generalized analytical expressions that more accurately describes some of the observed sickle cell shapes.

2. Materials and methods

Our benchtop SEFC system for imaging flowing cells [22] *in vitro* is illustrated in Fig. 1. Broadband light from a fiber-coupled super-luminescent diode array (Superlum Diodes, 840 nm central wavelength, 50 nm bandwidth) was collimated by an achromatic lens (L1, 11 mm focal length), 3-times magnified using an achromatic telescopic arrangement (L2 and L3), and focused onto a spectrally encoded transverse line using a transmission diffraction grating (1200 lines/mm, Wasatch Photonics), a unit magnification achromatic telescopic arrangement (L4 and L5), a dichroic mirror (680 nm cut-on wavelength) and a $60 \times$ water-immersion NA = 1.2 objective lens (L6, Olympus). Light reflected from the sample propagated back through the same optical path, deflected by a polarization-independent cubic beam splitter (BS) and focused (L7, 11 mm focal length) into a single-mode fiber (that also served as the confocal pinhole), and measured by a custom-built high-speed (up to 70k spectra/s) spectrometer. Lateral resolution was 0.7 μm, measured by imaging a reflective edge at the center of the field of view. Axial resolution (optical sectioning depth) was 1.9 μm (FWHM), measured by axial scanning of a reflective surface. Brightfield imaging of the cells was accomplished using transmission incoherent white-light illumination, an achromatic lens (L8, 50 mm focal length) and a monochrome camera (UI-2330SE, IDS, up to 78 frames/s). Venues blood samples from two patients (denoted patient #1 and patient #2, Institutional approval number 167-13) with homozygous sickle cell disease were collected into a vacutainer containing an anticoagulant. The blood was drawn from the vacutainer using a needle for minimal exposure to ambient oxygen in order to avoid undesired recovery of the cells back to their normal shapes [25]. The blood was then diluted within an eppendorf using phosphate buffered serum containing 2% fetal bovine serum, inserted into a syringe pump (Syringe pump 11 Elite, Harvard Apparatus) and pushed at a velocity of approximately 0.3 mm/s [26]. through a transparent plastic flow channel with a rectangular 5 mm x 0.1 mm cross section and a 0.17-mm-thick front wall.. The oxygenation level of the (venous) blood was approximately 70% [27] or lower, as expected from stored blood that may have lower pH compared to fresh blood [28]. Imaging experiments were performed in a temperature-regulated room (23°C) and under negligible shear forces due to the significant blood dilution and the wide flow channel.
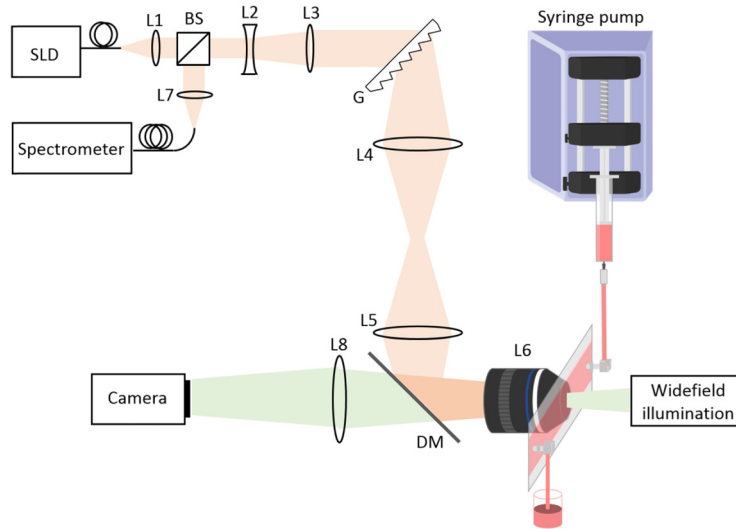
Fig. 1. Schematic of SEFC system for confocal imaging of flowing blood cells. SLD: super-luminescence diode array. L1-L8: Achromatic lenses. BS: beam splitter. G: diffraction grating. DM: dichroic mirror.

3. Results

A typical SEFC raw image of a diluted (1:25) blood sample from a sickle cell anemia patient #2 (Fig. 2) revealed different cell types, including white blood cells (w, most likely a neutrophil [20]), normal red blood cells (n), sickle cells (s), granular cells (g) and target-like cells (t). The normal RBCs often appear [22] as concentric interference rings and arcs; their shape is circular or elliptical with axes aspect ratios that depend on the flow velocity. The sickle cells, in contrast, appeared in various irregular elongated shapes characterized by sharp edges and non-uniform, often asymmetrical interference patterns. Many sickle cells also appeared brighter compared to most normal cells; however, additional detailed study would be required for verifying the extent and significance of this finding. Some abnormal cells appear spherical with jagged, non-smooth interference patterns, similar to what would be expected from granular cells (g). A few cells appeared with a bright spot at their center with external spherical circle and dim interference fringes; these cells may be similar to the well-known target cells (t) [29], whose membrane surface-to-volume ratios are abnormally high. High-resolution images (Fig. 3(a)-3(b)) of six selected sickle cells from the two patients provide a detailed view of the variety of cell shapes and their unique interference patterns. Images of three normal red blood cells from one of the patients are shown in Fig. 3(c), and brightfield images of the cells are shown next to each SEFC image, for reference. Most obvious in Fig. 3(a)-3(b) are the continuous, high-contrast interference patterns from the sickle cells, indicating that these cells maintain the smoothness, on a wavelength scale, of their plasma membranes.
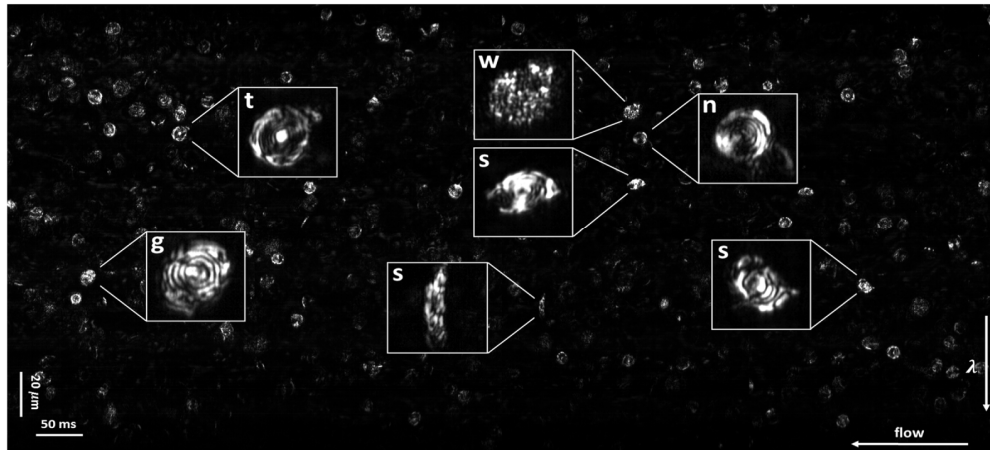
Fig. 2. Typical SEFC image of flowing blood cells. 5-times magnified views of selected cells are shown in the insets. w - white blood cell; n - normal red blood cell; s - sickle cell; g - granular cells; t - target-like cell.

Despite their characteristic irregular shapes, most of the cells show at least some circular interference patterns. Overall, approximately 30,000 and 100,000 individual blood cells were imaged from the blood samples of patient #1 and patient #2, respectively. Typically, within sixty seconds of continuous imaging, we have visually counted approximately 918 (9.94%) normal red blood cells, 144 (1.6%) sickle-shaped cells, 90 (1%) granular cells, 24 (0.26%) target cells, 96 (1%) leucocytes, and approximately 7962 (86.2%) cell fragments or cells that could not be easily classified into these groups.
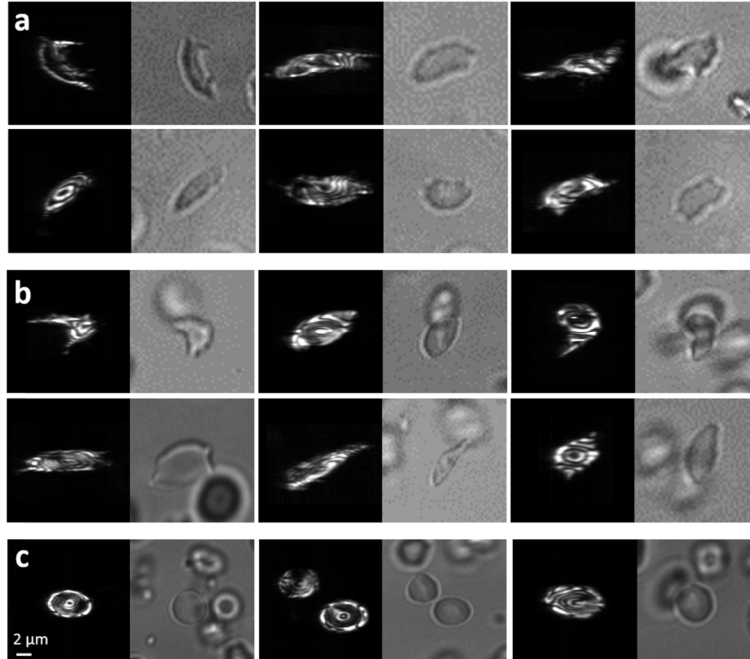

Fig. 3. Selected exemplary images of sickle cells obtained from (a) patient #1 and (b) patient #2. (c) Normal cells from patient #2. Left (right) hand panel of each pair of images corresponds to SEFC (brightfield) channel.

In order to study the three dimensional shape of individual sickle cells, we have developed a numerical simulation [22] of a reflectance confocal microscope, which uses the Fresnel approximation to calculate the resulting image from two reflecting membranes of arbitrary surface morphologies. The simulated numerical aperture was 0.6, chosen to match the experimentally measured axial resolution. For generating a numerical model of a sickle cell, we have first used an analytical expression that was derived by Lei and Karniadakis [23], in which the surfaces of the plasma membrane are approximated by the 4th-order polynomial:

$$f(x, y) = a_0 + a_1 x^2 + a_2 y^2 + a_3 x^4 + a_4 y^4 + a_5 x^2 y^2, \qquad (1)$$

and the cell boundaries in the lateral x-y plane are described by the Lame curves

$$\left(x/b_1 \right)^p + \left(y/b_2 \right)^p = 1. \qquad (2)$$

The parameters a_{0-5}, $b_{1,2}$ and p were chosen to best fit the top and bottom membrane surfaces of the specific cells that were imaged [23] using scanning electron microscopy (SEM). The interference patterns that would have resulted in our SEFC system using Eqs. (1) and (2) for typical [23] elongated, sickle and granular cells are shown in Figs. 4(a), 4(b) and 4(c), respectively. These simulated images contain only 1-3 relatively wide interference rings, notably less compared to the number of rings in the experimental SEFC images of the flowing cells, which showed between three and five dense fringes (see Fig. 3). Also, the corpuscular volume of the simulated cells using Eqs. (1) and (2), was 71 fL, somewhat lower than the typical mean corpuscular volume (MCV) of sickle cell anemia patients (75 fL − 95 fL) [30].
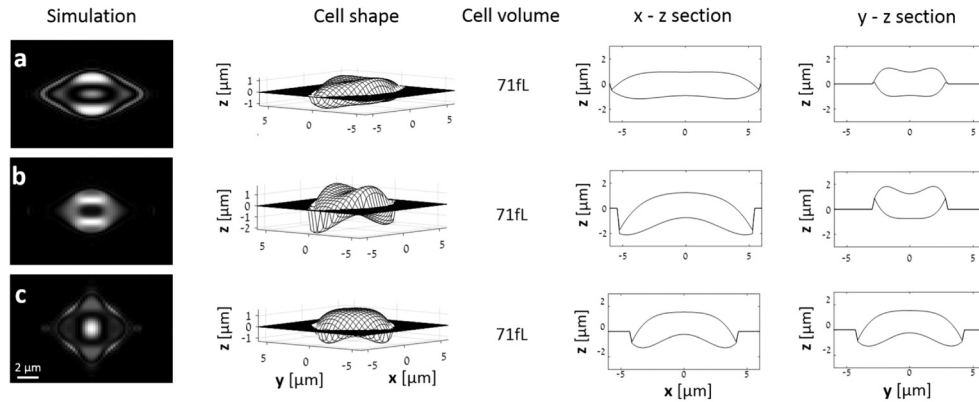

Fig. 4. Shape modeling according to ref (23) and the resulting simulated interference patterns. (a) Elongated cell. (b) Sickle cell. (c) Granular cell.

The multiple rings in our experimental images must have resulted from steep membrane curvatures that vary the separation between its two faces by at least several wavelengths; however, the polynomial in Eq. (1) do not have sufficient degrees of freedom to produce such variations. Specifically, Eq. (1) cannot describe a central dent in the cell membrane that appears to be comparable in depth to the characteristic dent at the center of normal cells [22,31]. A more accurate analytical representation of the cells, which generates the observed interference patterns in our SEFC images, required a separate expression for the indentation that is independent of the polynomial coefficients, for example by using multiplication by an inverted two-dimensional Gaussian

$$g(x, y) = \left(a_0 + a_1 x^2 + a_2 y^2 + a_3 x^4 + a_4 y^4 + a_5 x^2 y^2 \right) \left(1 - c_1 e^{-\frac{x^2}{c_2} - \frac{y^2}{c_3}} \right). \qquad (3)$$

Here, c_1 corresponds to the relative indention depth ($0 \leq c_1 \leq 1$), and c_2 and c_3 correspond to the indention width in the x and y axes, respectively. All nine parameters in Eq. (3) were carefully chosen to obtain the best fit to the experimental results. First, a_{0-5} were set to fit the general shape of the specific cell type (i.e. sickle, granular or elongated [23]), c_{2-3} where selected to match the width of the dent in the two horizontal axes, c_1 was chosen to match the dent relative depth, and a_0 was adjusted in discrete half-wavelength steps to obtain a physiological cell volume without significantly altering the simulated fringe pattern. After selecting all the parameters, an additional manual adjustment iteration was performed for each parameter to improve the visual matching between the theoretical and experimental interference patterns. Our numerical simulation and parameter fit using Eq. (3) yielded interference patterns (Fig. 5a) that more closely resemble the experimental results, when compared to using Eq. (1). Corpuscular volumes of the two simulated sickle cells in Fig. 5a were 83 fL and 88 fL, within the MCV normal range (75 fL - 95 fL) of sickle cell anemia patients [29]. The calculated interference patterns of the sickle cells modelled according to Eq. (3) fitted the experimental results well (based on visual qualitative inspection), where the elongated cells appear to maintain the characteristic biconcave membrane structure at their central region. An SEFC image and numerical simulation of a normal red blood cell is presented in Fig. 5b for reference.

4. Discussion and conclusions

The unique morphology of sickle cells is a result of hemoglobin polymerization at low oxygen saturation of the blood; the relatively stiff hemoglobin chains distort the symmetric disk-like shape of a normal erythrocyte into an elongated, nonsymmetrical shape. The wide variety of cell morphologies often results from the different polymerization conditions (oxygen level, temperature, mechanical stress, etc.) exhibited by each cell. Previous methods for characterizing sickle cell morphology [12,14,15] required static environments for enabling high-resolution imaging. Such methods often exert non-uniform stress on the cells membranes that distorts their shapes and prevents a reliable measurement. Similar to experiments with wide microfluidic channels [17], the nearly stress-free environment of the flowing cells in our experiments is more adequate for studying red blood cell morphology. The use of diluted blood not only allows for high-resolution imaging deep within the flow chamber, it also reduces the interaction between neighboring cells and thus permits a more consistent, artifact-free measurement. The use of scan-less optical confocal sectioning, provided in SEFC by the diffraction grating and the single-mode fibers, enabled high axial resolutions and allowed the formation of coherent interference patterns that yield additional information on the cell three-dimensional shapes.
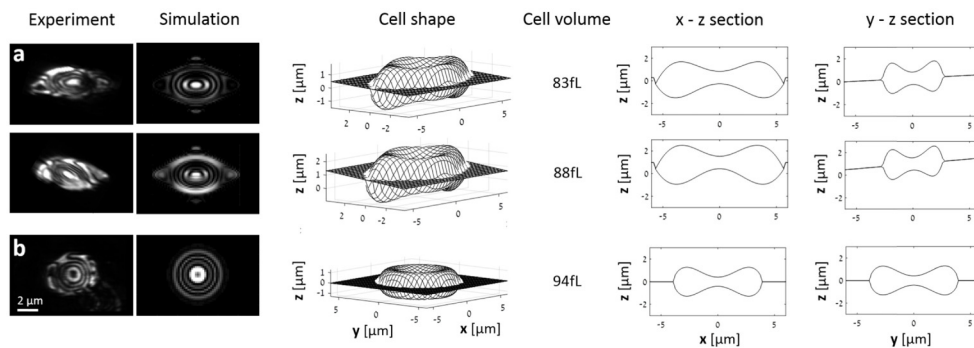

Fig. 5. Experimental images and simulated morphologies of (a) two elongated sickle cells and (b) a normal cell.

Our results reveal several interesting characteristics of the sickle cells. First, the smooth, continuous fringe structures in the SEFC images of the sickle cells indicates that they maintain optically smooth membranes, similar to normal erythrocytes, over large membrane surfaces. This implies that the hemoglobin polymerization inside the cells does not significantly alter the membrane surface at the wavelength (800 nm) scale, allowing the modeling of the membranes as smooth optically reflecting surfaces. Second, the numerous interference fringes in the SEFC images indicate that the sickle cells maintain the characteristic deep dent at their centers. This finding may imply that the cytoskeleton, which governs the membrane curvature [32], still plays a key role in preserving membrane structure. It may also suggest that the sickle cells, despite being altered into distorted shapes, maintain significant flexibility of their membranes that still tend to form curved surfaces for minimizing the total bending energy. The significant dent observed in the sickle cells could not be described using the 4th-degree polynomial suggested in Ref [23], most likely because it was derived for modeling cells that lost their characteristic dent during sample preparation for imaging by SEM, or because the cell images lacked sufficient axial resolution using conventional optical microscopy. Third, some of the cells with the characteristic sickle appearance appeared very bright, up to three times brighter than the normal red blood cells. While additional experiments with larger cell populations are required to confirm and study this phenomenon, the increased brightness may suggest that the refractive index of the plasma membrane or of the cytoplasm changes during the sickling process. Finally, some cells in the SEFC images were found to have a bright, circular appearance with a brighter than normal central spot (see the cell marked by the letter 't' in Fig. 2). It is yet unclear whether these cells are similar to the well-known 'target cells' that are commonly found in thalassemia patients [29].

Our approach for estimating cell shapes from the SEFC images is promising for studying both the morphology of red blood cells and their biomechanical properties under varying conditions. Additional study is required, however, in order to validate our method and develop its ability to provide an accurate, unambiguous shape measurement, for example, by imaging well-sorted cell populations or by imaging calibration test objects of various known morphologies. After system validation, future studies of sickle cell anemia would include imaging of various subpopulations of cells from anemia patients under a variety of experimental conditions, including a wide range of oxygenation levels, temperatures and shear forces. Biomechanical studies of sickle cells could also be conducted using imaging under different mechanical perturbations, for example by monitoring the instantaneous cells response to strong acoustic stimulations.

In summary, the three-dimensional morphology of sickle cells was studied using SEFC that provided high-speed, high-resolution reflectance confocal microscopy of the cells during flow. A new analytical model of the sickle cell shapes was developed using a fourth-degree polynomial multiplied by an inverted Gaussian function, which generates interference patterns that resemble the experimental images. The results suggest that the sickle cells often maintain their membrane smoothness and characteristic dent at the cell center. Future work is required to test the clinical diagnostics potential of this approach and to compare our *in vitro* results to *in vivo* imaging [21] in sickle cell anemia patients during sickle cell crisis.

Funding